

Prospects for studying million-degree gas in the Milky Way halo using the forbidden optical [Fe X] and [Fe XIV] intersystem lines

P. Richter¹, F. Runger¹, N. Lehner², J.C. Howk², C. Peroux^{3,4}, N. Libeskind⁵, M. Steinmetz⁵, and R. de Jong⁵

¹ Institut fur Physik und Astronomie, Universitat Potsdam, Karl-Liebknecht-Str.24/25, 14476 Golm, Germany

² Department of Physics and Astronomy, University of Notre Dame, Notre Dame, IN 46556, USA

³ European Southern Observatory (ESO), Karl-Schwarzschildstrasse 2, D-85748 Garching, Germany

⁴ Aix Marseille Universite, CNRS, LAM (Laboratoire d’Astrophysique de Marseille) UMR 7326, F-13388 Marseille, France

⁵ Leibniz-Institut fur Astrophysik Potsdam (AIP), An der Sternwarte 16, 14482 Potsdam, Germany

Received 2 June 2025; accepted 16 July 2025

ABSTRACT

Context. The Milky Way is surrounded by large amounts of hot gas at temperatures $T > 10^6$ K, which represents a major baryon reservoir.

Aims. We explore the prospects of studying the hot coronal gas in Milky Way halo by analyzing the highly forbidden optical coronal lines of [Fe X] and [Fe XIV] in absorption against bright (unrelated) extragalactic background sources.

Methods. We use a semi-analytic model of the Milky Way’s coronal gas distribution together with HESTIA simulations of the Local Group and observational constraints to predict the expected Fe X and Fe XIV column densities as well as the line shapes and strengths for the [Fe X] $\lambda 6374.5$ and [Fe XIV] $\lambda 5302.9$ transitions. We provide predictions for the signal-to-noise (S/N) ratio required to detect these lines. Using archival optical data from an original sample of 739 high-resolution AGN spectra from VLT/UVES and KECK/HIRES, we generate a stacked composite spectrum to measure an upper limit for the column densities of Fe X and Fe XIV in the Milky Way’s coronal gas.

Results. We predict column densities of $\log N(\text{Fe X}) = 15.40$ and $\log N(\text{Fe XIV}) = 15.23$ in the Milky Way’s hot halo, corresponding to equivalent widths of $W_{\text{FeX},6347} = 190 \mu\text{Å}$ and $W_{\text{FeXIV},5302} = 220 \mu\text{Å}$. We estimate that a minimum S/N of $\sim 50,000$ ($\sim 25,000$) is required to detect [Fe X] $\lambda 6374.5$ ([Fe XIV] $\lambda 5302.9$) absorption at a 3σ level. No [Fe X] and [Fe XIV] is detected in our composite spectrum, which achieves a maximum S/N = 1,240 near 5300 Å. We derive 3σ upper column-density limits of $\log N(\text{Fe X}) \leq 16.27$ and $\log N(\text{Fe XIV}) \leq 15.85$, in line with the above-mentioned predictions.

Conclusions. While [Fe X] and [Fe XIV] absorption is too weak to be detected with current optical data, we outline how up-coming extragalactic spectral surveys with millions of medium- to high-resolution optical spectra will provide the necessary sensitivity and spectral resolution to measure velocity-resolved [Fe X] and [Fe XIV] absorption in the Milky Way’s coronal gas (and beyond). This gives the prospect of opening a new window for studying the dominant baryonic mass component of the Milky Way in the form of hot coronal gas via optical spectroscopy.

1. Introduction

The dominant baryonic mass reservoir in galaxies is the diffuse gas contained within their halos. This so-called circumgalactic medium (CGM) plays a crucial role for the on-going formation and evolution of galaxies and thus has become a major research field in modern astrophysics (Tumlinson, Peeples & Werk 2017).

As a consequence of the highly complex physics (including the full magneto-hydrodynamics, cosmic rays, non-equilibrium cooling and heating) and the dynamics of the processes that contribute to the CGM’s mass and energy budget, the CGM is an extremely heterogeneous gaseous medium with multiple phases. In a simplified picture, the CGM is composed of cool and warm ($T = 10^2 - 10^5$ K) streams of gas that are embedded in a hotter gaseous medium ($T = 10^6 - 10^7$ K). As observations in the Milky

Way’s CGM show, the sizes of circumgalactic gas features range from AU scales (in high-density clumps; Richter, Sembach & Howk 2003; Meyer & Lauroesch 1999) to several hundred kpc (in large, coherent gas streams such as the Magellanic Stream; Putman 2003; Richter 2017). Only in the Milky Way can the CGM be observationally resolved at all these scales, making our Galaxy an important test ground for our general understanding of the circumgalactic medium. It is, on the other hand, this enormous dynamic range in physical conditions and spatial scales that makes it so challenging for magneto-hydrodynamical simulations to provide a realistic picture of CGM in all its facets (see Crain & van de Voort 2023, and references therein).

The global CGM properties of Milky Way type galaxies can be modeled in the context of Λ CDM galaxy formation models (White & Frenk 1991; Naab & Ostriker 2017), where it is predicted that diffuse gas in cosmological filaments is accreted onto dark matter halos and shock-heated to approximately the halo virial temperature (a few mil-

Send offprint requests to: P. Richter
e-mail: prichter@astro.physik.uni-potsdam.de

lion degrees for Milky-Way type galaxies). This hot gas is sometimes referred to as “galactic corona”, in analogy to the Sun’s hot coronal gas (Spitzer 1956). Cooling processes from the coronal gas, the stripping of satellite galaxies, and the accretion of metal-poor gas from the intergalactic medium (IGM) lead to the formation cold gas streams that move towards the disk where the gas is cooled and transformed into stars or is fueling the coronal gas of more massive galaxies (Afruni et al. 2023). In addition to accretion of material from the corona and from outside, gas (and energy) is also ejected into the CGM from inside from the disk as a result of feedback processes (Marasco et al. 2022) after which it is re-accreted onto the disk. Therefore, the CGM is believed to represent a substantial baryon reservoir that reflects the evolutionary state of its host galaxy (Péroux & Howk 2020).

With its low gas densities ($\log n_{\text{H}} = -2$ to -5 , typically) and high temperatures ($T > 10^6$ K), the hot coronal gas phase is particularly difficult to observe (Comparat et al. 2022). For the Milky Way, the X-ray transitions of O VII, O VIII and other high ions provide important diagnostic lines to study the Galaxy’s hot coronal gas component. These lines can be observed either in absorption against X-ray bright active galactic nuclei (AGN) or in emission (Fang et al. 2006; Miller & Bregman 2013, 2015; Hodges-Kluck et al. 2016; Li & Bregman 2017; Das et al. 2021). Recent X-ray studies indicate that the Milky Way’s hot coronal gas contains a total mass as much as $\sim 10^{11} M_{\odot}$ within 250 kpc (e.g., Miller & Bregman 2013, 2015). A major drawback of CGM X-ray observations is, however, the very low spectral resolution of the data that precludes a precise localization of the hot gas reservoirs within the Milky Way, its circumgalactic environment and in the Local Group (Bhattacharyya et al. 2023), giving only limited information on its overall dynamics.

Unlike in the X-ray band, there are no strong resonance lines from highly-ionized metals available in the ultraviolet (UV)/optical regime that would independently trace million-degree gas in the CGM and IGM at $z = 0$ in a direct manner. Indirect methods to trace hot gas in the local Universe in the CGM and IGM via intermediate-and high-resolution UV absorption spectroscopy include the measurements of transition-temperature gas ($T \sim 10^{5.5}$ K) using the O VI doublet (Sembach et al. 2003; Savage et al. 2003; Tripp et al. 2008) and the analysis of thermally broadened H I Ly α absorption lines (BLAs) and Coronal BLAs (CBLAs) that trace the tiny neutral gas fraction in the hot medium (Richter et al. 2006; Richter, Fang & Bryan 2006; Lehner et al. 2007; Tepper-García et al. 2012; Richter 2020). For the study of the CGM of the Milky Way and other Local Group member galaxies, the analysis of CBLAs is not an option, however, as the damped interstellar H I Ly α absorption superposes any CBLA signature within $|v_{\text{LSR}}| \approx 700$ km s $^{-1}$. High-ion transitions in the extreme UV, such as Ne VIII $\lambda\lambda 770.4, 780.3$, cannot be used to trace hot gas in the $z = 0$ Universe, but are accessible only at higher redshifts (Tepper-García, Richter & Schaye 2014).

A potential alternative to strong resonance lines are (exceedingly weak) forbidden transitions of high-ions, the most prominent of them (from early studies of the Sun) being located in the optical regime. Already in the 1980s, York & Cowie (1983) discussed the possibility to use the intersystem lines of [Fe X] near 6375 Å and [Fe XIV] near 5303 Å as the most promising candidate lines from the set of for-

bidden transitions in the optical regime to sample shock-heated, hot gas in the CGM and IGM in optical spectra from ground-based telescopes. However, because of the very small oscillator strengths of these forbidden transitions, an extremely high S/N of a few thousand would be required to detect these lines in the spectra of background AGN, which is (so far) not feasible for individual targets. In collisional ionization equilibrium, these lines trace gas at temperatures $T = 10^{6.0}-10^{6.3}$ K (see Fig. 1), thus close to the halo virial temperature of Milky-Way type galaxies (see above). In the 1980s, several groups searched for [Fe X] $\lambda 6374.5$ and [Fe XIV] $\lambda 5302.9$ absorption in the Milky Way ISM and in hot gas towards the LMC (Hobbs 1984a; Hobbs & Albert 1984; Hobbs 1985; Pettini & D’Odorico 1986; Wang, Hamilton & Helfand 1989; Pettini et al. 1989; Malaney & Clampin 1988), but none found a convincing signal (despite the initial claims of a detection; see discussion in Sect. 2.2). In complementing these optical studies, Anderson & Sunyaev (2016, 2018) have investigated emission signatures of hot gas around the nucleus of M87 using the highly forbidden transition of [Fe XXI] in the far UV at 1354.1 Å.

In Richter et al. (2014), we discussed the possibility of using the [Fe X] $\lambda 6374.5$ and [Fe XIV] $\lambda 5302.9$ lines in stacks of archival optical spectra of extragalactic sightlines from VLT/UVES to put constraints on the hot gas mass in the Milky Way coronal gas. There are several compelling reasons to seriously consider these transitions for a systematic study of the Milky Way’s hot coronal gas: i) detecting [Fe X] and/or [Fe XIV] would offer independent constraints on the mass of hot gas in and around the Milky Way, complementing other measurement methods; ii) acquiring the necessary data incurs no additional cost, as they will be readily available from numerous ongoing and upcoming extragalactic spectral surveys; iii) even deep optical surveys can provide relatively high spectral resolution, enabling detailed insights into the velocity profile of the absorbing gas, as well as its position relative to the Milky Way’s disk, central region, and large-scale environment - kinematic information that other methods cannot provide; iv) when combined with observations from other probes, such as Fast Radio Bursts (FRBs), these data may help to constrain the iron abundance in the Milky Way’s hot corona and shed light on the enrichment history of this gas. Zastrocky et al. (2018) stacked KECK/HIRES spectra from the KODIAQ sample to provide a first upper column-density limit for Fe XIV in the Milky Way halo; their limit is, however, more than two orders of magnitude above the expected level.

Motivated by the many upcoming spectroscopic galaxy surveys from other instruments, which will provide millions of medium- to high-resolution spectra, we revisit this idea and provide for the first time testable predictions for the expected strengths of the [Fe X] $\lambda 6374.5$ and [Fe XIV] $\lambda 5302.9$ absorption lines from the Galaxy’s hot coronal gas based on models, simulations, and observations of the distribution of the CGM in the Milky Way halo.

This paper is organized as follows: in Sect. 2, we review the physical properties of the [Fe X] $\lambda 6374.5$ and [Fe XIV] $\lambda 5302.9$ lines and discuss the results from previous attempts of detecting them. In Sect. 3, we discuss the hot gas distribution in the Milky Way halo and constrain the expected hot gas column density from an analytic model, from the HESTIA simulations of the Local Group, and from dispersion measurements. In Sect. 4, we make predictions for the expected absorption strength of these two lines and provide

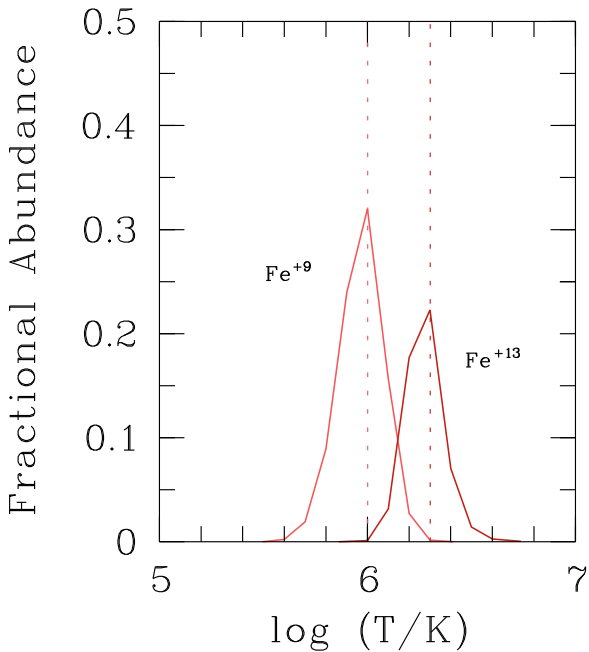


Fig. 1. Fractional abundances of Fe^{+9} and Fe^{+13} in a collisional ionization equilibrium (from Bryans, Landi & Savin 2009, see also Sect. 2.1).

upper limits for the column densities of $\log N(\text{Fe X})$ and $\log N(\text{Fe XIV})$ from a combined stack of VLT/UVES and KECK/HIRES. We discuss the prospects of detecting $[\text{Fe X}] \lambda 6374.5$ and $[\text{Fe XIV}] \lambda 5302.9$ absorption in stacked spectra from upcoming spectroscopic surveys in Sect. 5. Summary and conclusions are given in Sect. 6.

2. Tracing million degree gas with $[\text{Fe X}]$ and $[\text{Fe XIV}]$ absorption

2.1. Constraints from atomic physics

The optical intersystem transitions of $[\text{Fe X}]$ at $\lambda_0 = 6374.51 \text{ \AA}$ and $[\text{Fe XIV}]$ at $\lambda_0 = 5302.86 \text{ \AA}$ (Shirai et al. 2000)¹ are magnetic dipole transitions (M1) that are well known from observations of the solar corona, where these transitions lead to prominent emission features: the ‘‘coronal’’ lines, as known since 1939 (Grotrian 1939). In contrast to the high density ($n_{\text{H}} \sim 10^5 \text{ cm}^{-3}$) coronal plasma of the Sun, the forbidden optical intersystem transitions of $[\text{Fe X}]$ and $[\text{Fe XIV}]$ can be detected in the hot, low-density intergalactic and circumgalactic medium ($n_{\text{H}} < 10^{-4} \text{ cm}^{-3}$, typically) only in absorption against extragalactic background sources (such as quasars/quasi-stellar objects, QSOs, and other type of AGN).

The expected line strengths of $[\text{Fe X}] \lambda 6374.5$ and $[\text{Fe XIV}] \lambda 5302.9$ absorption in a given hot-gas distribution depend on i) the total gas column density, ii) the local iron abundance in the gas, iii) the fractional abundances of the Fe X and Fe XIV ions (e.g., dictated by the tempera-

ture in collisional ionization equilibrium), and iv) the transition probabilities (oscillator strengths) of the $\lambda 6374.5$ and $\lambda 5302.9$ transitions. In the following, we discuss all of these parameters and their relation to each other in preparation for our predictions of the $[\text{Fe X}]$ and $[\text{Fe XIV}]$ line strengths in the hot coronal gas of the Milky Way (Sect. 4.1).

The total column density, $N_{\text{tot}} \approx N(\text{H})$, of million degree coronal gas around the Milky Way (and other galaxies) has only partly been determined by X-ray observations (see introduction section), but can be estimated from analytic halo models and cosmological (magneto)hydrodynamical simulations as well as from measurements of the dispersion measure against extragalactic Fast Radio Bursts. This will be discussed in detail in Sect. 3.

The local iron abundance in the gas, $(\text{Fe}/\text{H})_{\text{Cor}}$, can be expressed in terms of the solar iron abundance $(\text{Fe}/\text{H})_{\odot} = 3.16 \times 10^{-5}$; Asplund et al. 2009), so that $(\text{Fe}/\text{H})_{\text{Cor}} \equiv X_{\text{Fe}}(\text{Fe}/\text{H})_{\odot}$ with X_{Fe} as free parameter to be defined. The fractional abundances of Fe X and Fe XIV in the gas, f_{FeX} and f_{FeXIV} , depend on the ionization state of the medium (and is thus driven by the ionization mechanisms). It requires very high energies of 234 eV to ionize Fe^{+8} to Fe^{+9} and 361 eV from Fe^{+13} to Fe^{+14} (e.g., Sutherland & Dopita 1993).

In the absence of an intense flux of extremely hard photons (as expected in most astrophysical environments and, in particular, in the CGM and IGM), collisional ionization at million-degree temperatures is the only mechanism that is expected to produce a significant population of Fe^{+9} and Fe^{+13} ions in diffuse intergalactic and circumgalactic gas. Assuming collisional ionization equilibrium (CIE), and adopting CIE models for Fe X and Fe XIV from Bryans, Landi & Savin (2009), the maximum fractional abundance of Fe X at its CIE peak temperature ($T_{\text{p,FeX}} = 1.0 \times 10^6 \text{ K}$) is $p_{\text{FeX}} = 0.32$, while for Fe XIV it is $p_{\text{FeXIV}} = 0.22$ at $T_{\text{p,FeXIV}} = 2.0 \times 10^6 \text{ K}$ (see Fig. 1). Note that these fractional abundances do not change significantly ($\Delta p \leq 0.002$) if one considers non-equilibrium collisional ionization models, such as presented in Gnat & Sternberg (2007). With Einstein coefficients of $A_{\text{ki}} = 69.4 \text{ s}^{-1}$ and $A_{\text{ki}} = 60.2 \text{ s}^{-1}$ (Fuhr, Martin & Wiese 1988), the transitions of $[\text{Fe X}] \lambda 6374.5$ and $[\text{Fe XIV}] \lambda 5302.9$ have extremely small oscillator strengths, $f_{\lambda 6374} = 2.1 \times 10^{-7}$ and $f_{\lambda 5302} = 5.1 \times 10^{-7}$.

For a weak, unsaturated absorption line of an ion Y , there is a simple, linear relation between the observed equivalent width, W_{λ} , and the ion column density, $N(Y)$, in the gas:

$$\left(\frac{W_{\lambda}}{\text{m\AA}}\right) = 8.85 \times 10^{-18} f \left(\frac{N(Y)}{\text{cm}^{-2}}\right) \left(\frac{\lambda_0}{\text{\AA}}\right)^2. \quad (1)$$

Here, λ_0 denotes the laboratory wavelength of the transition and f its oscillator strength.

At their respective CIE peak temperatures, the column densities of Fe X and Fe XIV then can be expressed as $N(\text{Fe X}) = p_{\text{FeX}} X_{\text{Fe}}(\text{Fe}/\text{H})_{\odot} N(\text{H}) = 1.01 \times 10^{-5} X_{\text{Fe}} N(\text{H})$ and $N(\text{Fe XIV}) = p_{\text{FeXIV}} X_{\text{Fe}}(\text{Fe}/\text{H})_{\odot} N(\text{H}) = 6.95 \times 10^{-6} X_{\text{Fe}} N(\text{H})$, so that

$$\left(\frac{W_{6347}}{\text{m\AA}}\right) = 0.0763 X_{\text{Fe}} \left(\frac{N(\text{H})}{10^{20} \text{ cm}^{-2}}\right) \quad (2)$$

and

$$\left(\frac{W_{5302}}{\text{m\AA}}\right) = 0.0882 X_{\text{Fe}} \left(\frac{N(\text{H})}{10^{20} \text{ cm}^{-2}}\right). \quad (3)$$

¹ Throughout this paper, we provide air-wavelengths in units \AA for the optical transitions of $[\text{Fe X}]$ and $[\text{Fe XIV}]$, as given in the NIST Atomic Spectra Database (Kramida et al. 2023), while we give vacuum wavelengths for transitions of UV lines at $\lambda \leq 3000 \text{ \AA}$.

We see that for a 1 mÅ absorption line to arise in the [Fe x] $\lambda 6374.5$ ([Fe xiv] $\lambda 5302.9$) line it requires a total ionized gas column density as large as $1.3 \times 10^{21} \text{ cm}^{-2}$ ($1.1 \times 10^{21} \text{ cm}^{-2}$) at a solar Fe iron abundance.

Because of the high gas temperature, the resulting absorption lines will be substantially broadened. The expected thermal Doppler parameter is

$$b_{\text{th}} = \sqrt{\frac{2kT}{m_{\text{ion}}}} \approx 0.129 \times \sqrt{\frac{T/\text{K}}{A_{\text{ion}}}} = 17 \text{ km s}^{-1} \left(\frac{T}{10^6 \text{ K}} \right). \quad (4)$$

In this equation, k is the Boltzmann constant, m_{ion} is the ion mass, and A is the relative atomic mass of the absorbing ion. In case of Fe, $A_{\text{Fe}} = 55.815$ (see NIST Atomic Spectra Lines Database; Kramida et al. 2023), so that for a gas temperature of $T = 10^6 \text{ K}$ ($2 \times 10^6 \text{ K}$) we have $b_{\text{th}} = 17 \text{ km s}^{-1}$ (24 km s^{-1}). Note that because of the relatively high mass of iron, this b_{th} value is substantially smaller than the b_{th} values expected for thermally broadened H I Ly α absorbers in the CGM ($A_{\text{H}} = 1$; Richter 2020). The expected small breadth of the Fe lines favours their detectability in a typical AGN continuum spectrum that is altered with noise features (see Fig. 2).

Because b_{th} is predicted to be relatively small for the Fe lines, non-thermal broadening mechanisms, e.g., from the differential co-rotation of the coronal gas with the disk and bulk motions of the hot gas, are expected to be important. Such non-thermal motions are commonly parameterized with b_{nth} , so that the expected observed Doppler parameter b is composed of both of these components, $b^2 = b_{\text{th}}^2 + b_{\text{nth}}^2$. The actual contribution of b_{nth} to b is challenging to estimate without knowing the systematic large-scale motions and the internal velocity dispersion of the hot gas in the corona.

There is observational evidence that the hot corona is partly co-rotating with the underlying disk (Hodges-Kluck et al. 2016). The implication of such a systematic motion along a line of sight from the Sun to Milky Way's virial radius for the shape of the Fe absorption lines is unclear, however, as it remains to be determined how the rotation speed scales with the vertical height of the hot gas layers. The role of non-thermal gas motions for b will be further discussed in Sect. 3.2, where we analyze the velocity dispersion of the coronal gas in the HESTIA simulations.

For a given equivalent width, the central absorption depth, \mathcal{D} , of an absorption line depends on its width and thus on b . Following Richter (2020), we can write (assuming a Gaussian shape):

$$\mathcal{D} = 0.139 \left[\frac{W_{\lambda}}{\text{mÅ}} \right] \left[\frac{b}{\text{km s}^{-1}} \right]^{-1}. \quad (5)$$

2.2. Previous [Fe x] and [Fe xiv] observations

In the light of the values obtained in the previous subsection, we now discuss the results from previous studies of [Fe x] and [Fe xiv] absorption in nearby hot gas and towards the Magellanic Clouds.

Already 40 years ago, (Hobbs 1984a; Hobbs & Albert 1984; Hobbs 1985; Pettini & D'Odorico 1986) searched for [Fe x] and [Fe xiv] absorption in the local Milky Way ISM using high S/N spectra of nearby stars. These studies did not find any convincing signal down to a level of $\sim 1 \text{ mÅ}$.

However, million-degree gas within the Milky-Way gas disk is expected to reside only in localized environments at sub-kpc scales (e.g., the local hot bubble or other supernova bubbles and chimneys) that do not provide sufficient column density for [Fe x] and [Fe xiv] absorption to be detected at a $\sim 1 \text{ mÅ}$ level (e.g., Liu et al. 2017). This is because for a hot-gas density as high as $n_{\text{H}} = 10^{-2} \text{ cm}^{-3}$, it requires an absorption path length of 3.2 kpc to achieve a hydrogen column density of $N(\text{H}) = 10^{20} \text{ cm}^{-2}$. Therefore, the reported non-detections in the above-listed studies are consistent with equations (2) & (3).

From the analysis of the optical spectrum of the extremely bright supernova SN 1987A in the LMC, several groups (Wang, Hamilton & Helfand 1989; Pettini et al. 1989; Malaney & Clampin 1988) reported the detection of a weak ($W_{\lambda} \sim 3 \text{ mÅ}$) absorption feature near 6380 Å that was identified as Doppler-shifted [Fe x] $\lambda 6374.5$ absorption arising from hot gas in the direction of the LMC (Pettini et al. 1989). If true, this would imply a large column of ionized gas in this direction, $\log N(\text{H II}) \approx 21.5$ (Eq. 2), indicating the existence of a huge reservoir of baryonic matter hidden in hot gas. The interpretation of the observed absorption feature near 6380 Å as [Fe x] absorption was, however, disputed by Wampler, Chen & Setti (1991), who identified the observed feature as a Doppler-shifted diffuse interstellar band (DIB). There are several weak DIBs and telluric lines present in the optical regions in which the [Fe x] $\lambda 6374.5$ and [Fe xiv] $\lambda 5302.9$ lines are located (see, e.g., Jenniskens & Desert 1994). The latter interpretation appears more likely, because the existence of a uniform layer of million-degree gas around the LMC at a column density of $\log N(\text{H II}) \approx 21.5$ would imply an enormously high baryon-to-dark-matter ratio that is not in line with current galaxy formation models. Such a large ionized gas column density is also not supported by UV and X-ray observations of hot gas in the general direction of the LMC (Krishnarao et al. 2022; Locatelli et al. 2024).

More recently, Richter et al. (2014) discussed high S/N VLT/UVES observations of high-redshift QSOs as possible probes for [Fe x] and [Fe xiv] absorption in the Milky Way's coronal gas (e.g., their Fig. 4). They also proposed stacking techniques for UVES high-resolution and SDSS low-resolution archival spectra to achieve the required S/N levels. From the stacking of 95 pre-selected Keck HIRES spectra, Zastrocky et al. (2018) derived 3σ upper limits for [Fe xiv] absorption in the Milky Way halo of $W_{5302} \leq 7 \text{ mÅ}$ and $N(\text{Fe xiv}) = 5.5 \times 10^{16} \text{ cm}^{-2}$ achieving a S/N of ~ 300 .

3. Expected properties of the Milky Way's hot coronal gas

To determine realistic expectation values for W_{6347} and W_{5302} from [Fe x] and [Fe xiv] absorption in the Milky Way's hot coronal gas, we need to estimate $N(\text{H})$ for the coronal gas at the CIE peak temperatures of Fe^{+9} to Fe^{+13} (Fig. 1) in the range $\log T = 6.0 - 6.3$ (see Eqs. 2 and 3) for extragalactic sightlines from the vantage point of the Sun. For this, we use i) the semi-analytic model of the hot gas distribution around low-redshift galaxies from Richter (2020), ii) results from the constrained magneto-hydrodynamical simulation of the Milky Way and Local Group as part of the HESTIA project (Libeskind et al. 2020; Damle et al.

2022; Runger et al. 2025), and iii) constraints from measurements of the dispersion measure of gas in around the Milky Way using Fast Radio Bursts (Cook et al. 2023).

3.1. Constraints from a semi-analytic model

In Richter (2020), we used a semi-analytic approach to model the spatial density and temperature distribution of hot coronal gas of galaxies with virial halo masses in the range $\log(M/M_\odot) = 10.6 - 12.6$ to predict strength, spectral shape, and cross section of the CBLAs as a function of galaxy-halo mass and line-of-sight impact parameter from an external vantage point. In this model, it is assumed that the hot coronal gas is confined in a dark-matter halo that follows a Navarro–Frenk–White (NFW) density profile (Navarro, Frenk & White 1995; Klypin et al. 2001). After the initial collapse, the gas is assumed to be shock-heated to the halo’s virial temperature and then cools within a characteristic cooling radius to become multi-phase (see Maller & Bullock 2004, for a detailed description of the original equations).

To model the spectral signatures of such gas along QSO sightlines, we then have applied the `halopath` code, as originally described in Richter et al. (2012). The same approach and modeling codes is used here to calculate $N(\text{H})$ for $T \geq 10^6$ K in a Milky-Way mass halo from any given vantage point inside the halo by integrating n_{H} from the initial position out to the virial radius, R_{vir} .

For the Milky Way mode halo, we adopt a halo mass of $\log(M/M_\odot) = 12.0$ and a virial radius of $R_{\text{vir}} = 250$ kpc and for sake of simplicity we assume the observer to be located in the geometrical center of the spherical model halo (for more details about the model see Richter 2020). If we only consider gas with $T \geq 10^6$ K, the total hydrogen column density of that gas between $R = 0$ kpc and R_{vir} is typically $N(\text{H I}) = 1.0 \times 10^{20} \text{ cm}^{-2}$. To put this number into context: a similar column density is observed for neutral hydrogen in the Magellanic Stream (e.g., Putman 2003; Fox et al. 2013; Richter et al. 2013), where the absorption path-length through the stream is substantially smaller (a few kpc, at most), but the gas density is significantly higher (as is the neutral gas fraction) as well as in the lowest $N(\text{H I})$ directions in the Milky Way disk, such in the Lockman hole (Richter et al. 2001).

3.2. Constraints from the HESTIA simulations

While the semi-analytic halo model discussed above provides important insights into the overall hot gas distribution in the CGM as a function of halo mass, it cannot deliver information on the kinematics of the absorbing gas cells, nor can it account for density and temperature fluctuations in the hot CGM that are expected to arise due to the specific cosmological environment of the host galaxy and because of feedback processes from supernovae and AGN activity. Therefore, for a more realistic estimate of $N(\text{H})$ in the hot CGM of a Milky-Way type galaxy, we consider magneto-hydrodynamical (MHD) high-resolution simulations of galaxies in a cosmological context.

We make use of the suite of simulations from the HESTIA (High-resolution Environmental Simulations of The Immediate Environment) project (Libeskind et al. 2020) to systematically investigate the properties of the (simu-

lated) Milky Way CGM (Damle et al. 2022; Biaux et al. 2022; Runger et al. 2025). HESTIA provides representative magneto-hydrodynamical simulations of Milky Way-mass galaxies in their proper cosmographic environments using the AREPO moving-mesh code (Springel et al. 2010) and the AURIGA galaxy evolution model (Grand et al. 2017). For details on HESTIA, see Libeskind et al. (2020).

We here use the three HESTIA simulations to estimate $N(\text{H})$ in the coronal gas from a Sun-like position at 8 kpc galactocentric distance within the (simulated) MW disk and pinpoint the velocity dispersion of the hot-gas pockets in the CGM along the various sightlines to constrain the non-thermal contribution to the Doppler parameter (Sect. 2.1). For each of the three MW simulations, we have constructed 100 randomly distributed sightlines from the position of the Sun that extend to R_{vir} and derived $N(\text{H})$ by integrating over the density distribution along each sightline. As for the semi-analytic model, we restrict our analysis to gas with temperatures $T \geq 10^6$ K. The median value for $N(\text{H})$ from all 300 sightlines is $N(\text{H}) = 5 \times 10^{20} \text{ cm}^{-2}$. Interestingly, this value is ~ 5 times higher than $N(\text{H})$ estimated from the simple semi-analytic model (Sect. 3.1). The larger column density of hot, ionized gas in the HESTIA simulation comes from the important contributions of hot gas cells related to the Milky Way’s (simulated) disk-halo interface, where supernova feedback adds to the energy and hot-baryon budget of gas in the lower halo, and possibly from gas related to Milky Way satellites within R_{vir} (see also Damle et al. 2025).

The (radial) velocity dispersions of the hot gas cells along the 300 sightlines vary between 30 and 128 km s^{-1} with a median value of $\langle \sigma_v \rangle = 50 \text{ km s}^{-1}$. We regard this latter value as a characteristic velocity dispersion for the non-thermal gas motions along a typical halo sightline, which then dominates expected line width of the $[\text{Fe X}]$ and $[\text{Fe XIV}]$ absorption (Sect. 2.1).

3.3. Constraints from Fast Radio Bursts

Another, independent constraint on the mass and extent of the hot gas in the the Milky Way halo comes from FRBs (Lorimer et al. 2007) and distant pulsars, using the well-known dispersive effect of charged particles on radio waves. By precisely measuring the arrival times of radio pulses (e.g., from pulsars or FRBs), the dispersive delay can be quantified using a quantity called the dispersion measure (DM). Since free electrons by far dominate the dispersion in a given ionized gas volume, the DM is proportional to the electron column density in the gas along a line of sight of length L ,

$$\text{DM} = \int_0^L n_e dl = N(e^-). \quad (6)$$

And because hydrogen is the main electron donor in a fully ionized interstellar/intergalactic plasma at solar or sub-solar metal abundance, we have $N(e^-) \approx N(\text{H})$, so that the DM is a direct measure of the total (ionized) gas mass along a line of sight.

DM measurements deliver information on the total ionized gas column towards a background FRB or pulsar. They do not, however, provide any information on how the particles are distributed along the line of sight. To localize hot gas in and around the Milky Way and estimate its mass,

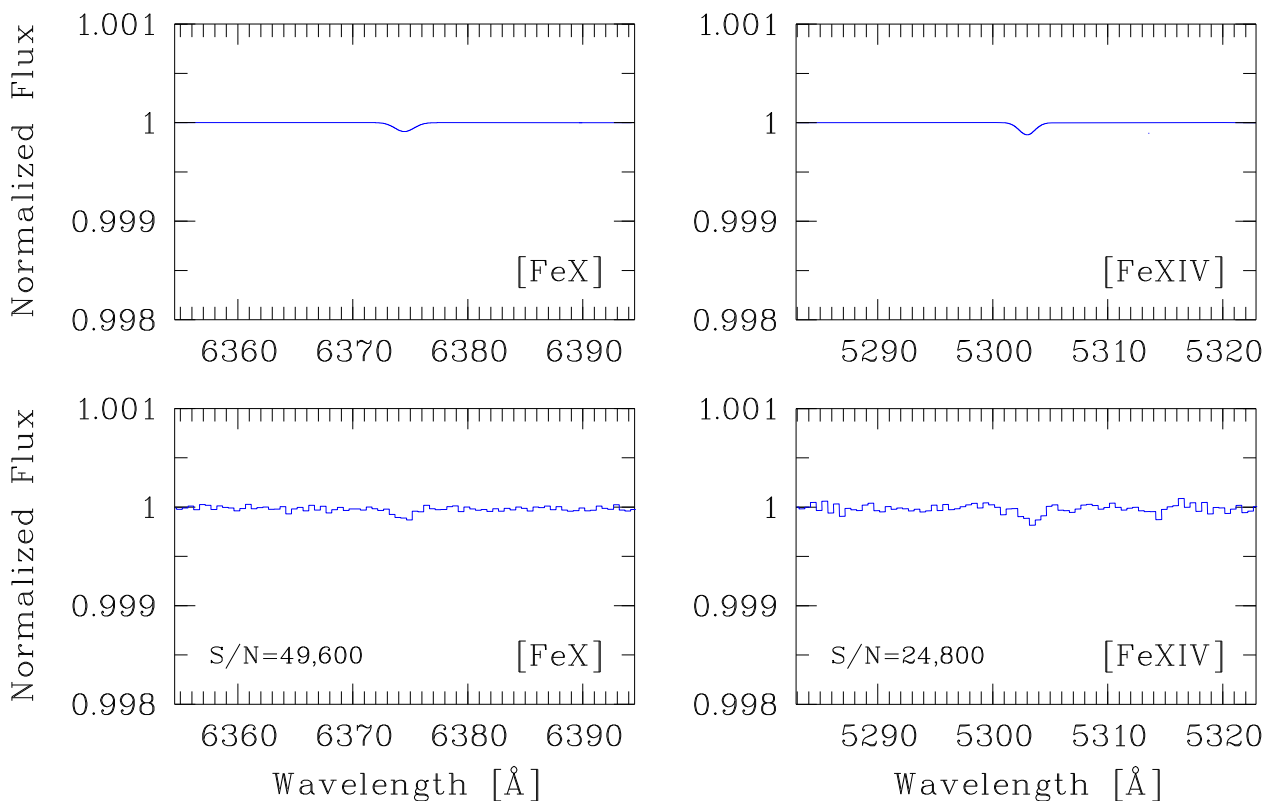


Fig. 2. Synthetic spectra of the [Fe X] at $\lambda 6374.5$ and [Fe XIV] $\lambda 5302.9$ lines from our halo model described in Sect. 4.1. The upper two panels show the noise-free absorption profiles, the lower two panels show the profiles with the minimum S/N required for a 3σ detection, as given in the lower left corners. The spectra are generated using a spectral resolution of $R = 45,000$ and a sampling of 1.5 pixels per resolution element.

the combination of many FRB and/or pulsar sightlines of different lengths is required (see, e.g., Prochaska & Zheng 2019). From a sample of 93 FRBs for Galactic latitudes $|b| \geq 30$ deg from the CHIME/FRB project, Cook et al. (2023) derived a range of $DM = 88 - 141$ pc cm^{-3} . These values correspond to a range in total ionized gas column densities of $N(\text{H}) = 2.7 - 4.4 \times 10^{20} \text{cm}^{-2}$, thus slightly below the value estimated from the HESTIA simulations, but clearly above the one derived from the semi-analytic model.

4. Observational limits

4.1. Expected line strengths and profiles

If we assume a total hydrogen column density in the Milky Way’s hot coronal gas of $N(\text{H}) = 5 \times 10^{20} \text{cm}^{-2}$ and an iron abundance in the corona of half of the solar value (Martylenko 2022), the expected line strengths from equations (2) and (3) come out as $W_{6374} = 190 \mu\text{Å}$ and $W_{5302} = 220 \mu\text{Å}$. The corresponding Fe X and Fe XIV column densities are $\log N(\text{Fe X}) = 15.40$ and $\log N(\text{Fe XIV}) = 15.23$. For a hot-gas temperature of 2×10^6 K and non-thermal gas motions characterized by $b_{\text{nt}} = 50 \text{km s}^{-1}$ (from the HESTIA simulations, see above), the expected total Doppler parameter is $b = 58 \text{km s}^{-1}$.

To visualize the optical appearance of such weak spectral features, we have generated synthetic spectra of the [Fe X] $\lambda 6374.5$ and [Fe XIV] $\lambda 5302.9$ lines in Fig. 2 using a spectral resolution of $R = 45,000$ and a sampling of 1.5 pixels per resolution element. The upper two panels show

the blank (noise-free) absorption profiles, for the lower two panels we have added noise at a level, that a 3σ detection of these features is realized. As we can see, a S/N of $\sim 50,000$ is required to significantly detect [Fe X] absorption at the expected level, for [Fe XIV] it is $\sim 25,000$.

4.2. Stacking of archival high-resolution optical AGN spectra

Even with the most efficient spectrographs on 8 – 10m class telescopes, it is unrealistic to achieve the required S/N of $> 20,000$ for a medium- to high-resolution ($R \geq 15,000$) optical spectrum of an individual extragalactic background source within reasonable integration times. For the UVES spectrograph, for instance, D’Odorico et al. (2016) and Kotuš, Murphy and Carswell (2017) presented high-resolution ($R \geq 45,000$) spectra of the high-redshift QSOs HE 0940–1050 and HE 0515–4414, respectively. These data have S/N ratios of $\sim 500 - 600$ per resolution element and are based on many individual pointings totaling several dozen hours of integration time with the VLT. To our knowledge, there are no other VLT/UVES (or KECK/HIRES) spectra of an individual QSO that provide a S/N significantly higher than these values.

Because every extragalactic sightline passes the Milky Way halo, however, stacking clearly is the most promising approach to achieve S/N ratios larger than 1000 for a Milky Way composite spectrum. Using low-resolution ($R \sim 2,200$) SDSS spectral data from stars, galaxies and quasars, Lan, Ménard & Zhu (2013) and Murga et al. (2013) have achieved a S/N of several thousand by stacking a few

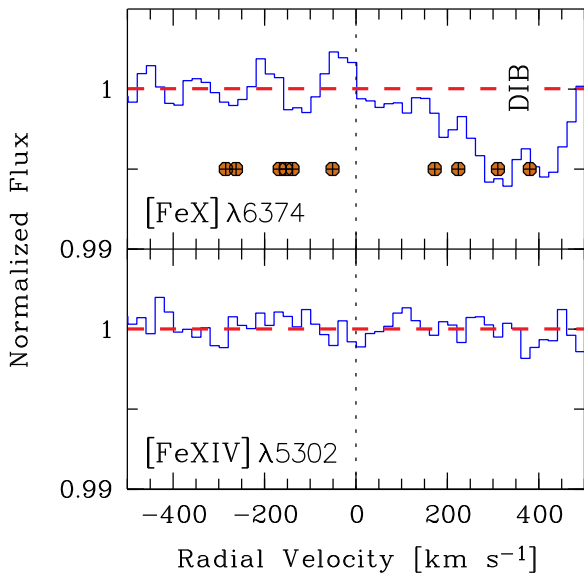


Fig. 3. Velocity profiles from stacks of the [Fe x] $\lambda 6374.5$ and [Fe xiv] $\lambda 5302.9$ lines from a combined sample of 186/156 VLT/UVES and KECK/HIRES spectra (see Sect. 4.2). The resulting S/N per 20 km s^{-1} pixel element is 900 for the stacked [Fe x] profile and 1,240 for [Fe xiv]. In the profile of the [Fe x] line, a weak DIB is detected near $+300 \text{ km s}^{-1}$. The positions of telluric features in the [Fe x] profile are indicated with the crossed circles (from Pettini et al. 1989). Note that the S/N ratios achieved here still are 1 – 2 orders of magnitude below the values predicted by our models (see Fig. 2).

hundred thousand SDSS spectra to investigate interstellar DIBs and Ca II absorption in the Milky Way foreground gas. They did not, however, find evidence for [Fe x] and [Fe xiv] absorption in their stacked data set (Menard, priv. comm.; see also Lan, Ménard & Zhu 2013, their Fig. 2), which is in line with the predicted strength of the absorption as calculated above. We also note that the spectral resolution of SDSS ($R = 2200 - 2850$, equivalent to $\Delta v \geq 136 \text{ km s}^{-1}$) is not sufficient to resolve the two [Fe x] and [Fe xiv] lines at the expected widths.

Zastrocky et al. (2018) used a sample of 95 KECK/HIRES spectra from the KODIAQ survey (O’Meara et al. 2017) for a spectral stack to search for [Fe xiv] absorption in the Milky Way halo. They achieve a S/N of ~ 300 and a column density limit of $\log N(\text{Fe xiv}) \leq 16.78$ from the mean stack of their composite spectrum, which is far below (two orders of magnitude in terms of S/N) the required sensitivity.

For this paper, we have combined the KECK/HIRES spectra from the KODIAQ data basis with VLT/UVES spectra from the SQUAD project (Murphy et al. 2019) and other archival VLT/UVES data. Our goal is to boost the detection limit for [Fe x] and [Fe xiv] absorption from a high-resolution composite spectrum that is based on high-quality data from two of the most powerful optical spectrographs installed on 8 – 10m class telescopes currently available. Both spectral data sets have similar spectral resolution $R \sim 30,000 - 60,000$, but the average S/N in the VLT/UVES spectral data is 2 – 3 times higher than for the KECK/HIRES data including some spectra with exceptionally high S/N (see above) from the monitoring of AGN variability. Note that we have previously used VLT/UVES

spectra from the SQUAD project to systematically investigate Ca H & K absorption in the Milky Way halo (Richter, Westmeier & Brüns 2005; Ben Bekhti et al. 2008, 2012), in the low-redshift IGM (Richter et al. 2011), and in selected Damped Lyman- α absorbers (Guber & Richter 2016; Guber, Richter & Wendt 2018). We therefore are highly familiar with the data quality issues of the SQUAD database.

For the stacking, we developed a custom stacking routine that (in a fully automated fashion) identifies blending features from intervening absorbers in the spectral regions near 5300 and 6375 Å, performs data quality checks, and determines the local S/N. Using pre-defined selection criteria and bin sizes, the code then bins the data and stacks the selected spectra, where each spectrum is weighted by the inverse variance from the noise statistics in the regions around the two Fe lines. In our case, the initial sample contains 439 UVES and 300 HIRES spectra (i.e., 739 in total). Before stacking, we pre-selected spectra that i) have no contaminating blending line within $\pm 500 \text{ km s}^{-1}$ of the laboratory wavelength of the [Fe x] and [Fe xiv] lines, and ii) that (each) have a $S/N \geq 20$ per resolution element. This selection leaves us with 183 spectra for [Fe x] and 156 spectra for [Fe xiv] to carry out the stacking procedure. Before stacking, the individual spectra were re-binned to achieve a homogeneous sampling, where the bin size was chosen to be 20 km s^{-1} , sufficient to resolve an absorption line that has an expected Doppler parameter of $b \geq 50 \text{ km s}^{-1}$. Finally, the stacked spectrum was normalized in the regions of interest using a linear continuum fit. The resulting composite velocity profiles for the [Fe x] and [Fe xiv] lines after stacking are shown in Fig. 3.

For [Fe xiv] (lower panel), the stacked composite at 5302 Å is featureless and achieves a very high $S/N = 1,240$ per 20 km s^{-1} wide pixel element, which translates into a 3σ upper equivalent-width limit of $W_{5302} \leq 0.9 \text{ mÅ}$ and $\log N(\text{Fe xiv}) \leq 15.85$.

For [Fe x] (upper panel), the composite spectrum is slightly noisier between -500 and $+200 \text{ km s}^{-1}$ ($S/N = 900$), corresponding to a 3σ upper equivalent-width limit of $W_{6374} \leq 1.4 \text{ mÅ}$ and $\log N(\text{Fe x}) \leq 16.27$. There are a number of telluric features known in the spectral region between 6365 and 6385 Å (see Table 2 in Pettini et al. 1989) that could potentially contaminate any [Fe x] $\lambda 6374.5$ absorption. Their positions are indicated in Fig. 3. The [Fe x] profile also shows an absorption feature at a ~ 0.5 percent absorption-depth level between $+250$ and $+450 \text{ km s}^{-1}$. This feature represents a DIB at 6379.32 Å (Jenniskens & Desert 1994) and is well-known from Galactic stellar sightlines with high extinction (e.g., Hobbs et al. 2008, their Fig. 3). It is also identified at a ~ 0.5 percent level in a stack of more than 40,000 SDSS spectra of Galactic stars along sightlines with $E(B - V) > 0.1 \text{ mag}$ (Lan, Ménard & Zhu 2013).

In our [Fe x] composite spectrum, we measure an equivalent width of 29.5 mÅ for this feature. The fact that this DIB emerges in our stacked composite spectrum of extragalactic AGN sightlines, which are predominantly located at high Galactic latitudes, strongly supports the conclusion that the feature near 6380 Å in the spectrum of SN1987A in the LMC is caused by the DIB at 6379.32 Å and not by [Fe x] absorption from hot coronal gas (see discussion in Sect. 2.2). The detection of this feature in our composite

spectrum also demonstrates the robustness of our stacking procedure.

In conclusion, our stacking experiment suggests that the [Fe X] $\lambda 6374.5$ line in composite spectra is usable only within a limited velocity range of -50 and $+150$ km s^{-1} due to potential blending with a DIB and telluric features. In contrast, the [Fe XIV] $\lambda 5302.9$ line offers a more promising alternative, as it is unaffected by such blending, allowing the full velocity range of the Milky Way to be explored.

5. Outlook

5.1. General prospects from future spectroscopic surveys

While the current archival spectral data base is insufficient to reach the required S/N to obtain meaningful constraints on [Fe X] and [Fe XIV] in the Milky Way’s coronal gas via stacking, the prospects from observational surveys in the near future are excellent. With the advent of several new survey instruments and the installation of extremely sensitive optical telescopes such as the ESO Extremely Large Telescope (ELT; eso.org), there soon will be several millions of spectra available at medium- to high spectral resolution that will open completely new windows to search for extremely weak absorption features of various ions in the foreground gas in the Milky Way’s interstellar and circumgalactic medium (D’Odorico et al. 2024).

Fresco et al. (2020) have explored in detail the prospects of using future spectroscopic surveys to investigate hot gas at $\sim 10^7$ K around damped Ly α absorbers in the early Universe by stacking a large number of optical spectra. Their goal is to put constraints on the absorption strength of the red-shifted forbidden [Fe XXI] $\lambda 1354.1$ UV line (Anderson & Sunyaev 2016) in the hot gas around these (proto-)galactic structures at median redshift of $\langle z_{\text{abs}} \rangle = 2.5$. In their paper, the authors discuss the instrumental capabilities of future spectroscopic surveys with millions of optical spectra from projects including i) the Multi-Object Spectrograph Telescope (4MOST), a high-multiplex spectroscopic survey instrument for the 4m VISTA telescope at ESO (de Jong 2019; Mainieri et al. 2023), for which science operations expected to starting in mid-2026; ii) the WEAVE instrument (Jin et al. 2024), designed for the William Herschel Telescope (WHT), which had first light in Dec 2022, and iii) the AmazoNES high Dispersion Echelle Spectrograph (ANDES; formerly named HIRES), which will be installed on 39m Extremely Large Telescope (ELT) currently under construction (Marconi et al. 2022; D’Odorico et al. 2024). For details of these instruments and their performance in the context of stacking experiments we refer to the discussion in Fresco et al. (2020).

The search for redshifted [Fe XXI] absorption around high- z DLAs, such as described in Fresco et al. (2020), is not only limited by the number of high-redshift ($z > 2.2$) background quasars, but also by the cosmological number density (e.g., cross-section) of these absorbers. By contrast, every extragalactic sightline passes the hot coronal gas of the Milky Way, boosting the number of available spectra for stacking experiments using [Fe X] and [Fe XIV] and other weak absorption features in the Galaxy’s CGM and ISM.

Achieving a S/N as high as 25,000 in a spectral stack, as estimated for the [Fe XIV] line in Sect. 4.2, will be extremely challenging, however. Depending on the type of background sources (e.g., AGN, galaxy, star) and their redshift distri-

Table 1. Predictions for detecting [Fe XIV] in future surveys

$\langle \text{S/N} \rangle^{\text{a}}$	$\mathcal{N}_{\text{stack}}^{\text{b}}$
10	6.3×10^6
25	1.0×10^6
50	2.5×10^5
100	6.3×10^4

^a Average S/N per 50 km s^{-1} wide bin element in individual spectra;

^b Number of usable spectra for stacking.

bution, only a certain fraction of the available spectra can be used for a stack in the [Fe X] and [Fe XIV] wavelength region due to blending effects and continuum issues. For our VLT/UVES sample described in Sect. 4.2, for example, this fraction comes out to 20 – 25 percent.

In Table 1, we list the minimum number of usable spectra, $\mathcal{N}_{\text{stack}}$, required to reach a S/N of 25,000 per 50 km s^{-1} wide bin element (second column) as a function of the average S/N per bin in the spectral sample. For a reliable estimate for $\mathcal{N}_{\text{stack}}$, one needs to know the overall sample size of available sources, their exact type and redshift distribution as well as their S/N distribution. The actual S/N achieved from a mix of possible instruments and background sources would also need to be evaluated from a large set of mock spectra with properties similar to those of the real data.

5.2. Example: potential stacking experiments with 4MOST data

In the following, we elaborate more on the scientific potential of up-coming spectral surveys for [Fe XIV] stacking experiments by focussing on the 4MOST instrument (de Jong 2019). Designed as a high-multiplex spectroscopic survey instrument for the 4m VISTA telescope at ESO, 4MOST has both a Low-Resolution Spectrograph (LRS; $R \approx 5,600$ at 5302 \AA , corresponding to $\Delta v = 53.5 \text{ km s}^{-1}$) and a High-Resolution Spectrograph (HRS; $R \approx 19,000$ at 5302 \AA , corresponding to $\Delta v = 15.8 \text{ km s}^{-1}$). In principle, the spectral data from both of these instrumental setups therefore can be used for [Fe XIV] stacking experiments. 4MOST is expected to deliver LRS and HRS data for several million extragalactic sources (AGN and galaxies) as part of the Extragalactic Consortium Surveys (e.g. Richards et al. 2019; Merloni et al. 2019) and the Extragalactic Community Surveys (e.g. Bauer et al. 2023; Péroux et al. 2023) covering a broad range of S/N ratios. With such a rich data set, it hopefully will be possible to constrain the mean [Fe XIV] column density in the Milky Way disk and halo and estimate the total amount of million-degree gas in our Galaxy.

As mentioned above, the biggest advantage of using stacked optical spectra compared to X-ray observations and studies of the dispersion measure lies in the (relatively) high spectral and radial-velocity resolution of optical spectrographs (even in their “low-resolution” modes). Also a moderate velocity resolution of $\Delta v \approx 50 \text{ km s}^{-1}$ will be sufficient to explore the radial velocity profile of the hot gas in and around the Milky Way and to estimate its mass as a function of distance to the Sun.

If sufficient S/N can be achieved even with spectral subsamples, it may also be possible to investigate the patchiness of the hot gas in the Milky Way on angular scales

(see Kaaret et al. 2020) and - together with the velocity information- to localize the hot gas reservoirs in the inner and outer Milky Way halo, such in the disk-halo interface (Savage et al. 2003) and in the extra-planar regions influenced by the Galaxy’s nuclear outflow (“eROSITA bubbles”, Predehl et al. 2020; Sarkar 2024). Such data may also provide important information on the possible co-rotation of the hot halo with the underlying disk, as proposed by Hodges-Kluck et al. (2016) based on low-resolution X-ray data.

Because of its relatively large angular extent (Richter et al. 2017, their Fig. 8) and its substantial radial velocity offset from the Milky Way (300 km s^{-1}), also the extended corona of M31 might be a potential target for a [Fe XIV] stacking experiment using extragalactic sightlines in the direction of the Local Group barycenter (see also Lehner, Howk & Wakker 2015; Lehner et al. 2020). Such observations also could be coupled to FRB measurements to constrain $N(\text{Fe})/N(\text{H})$ and thus the metallicity of the coronal gas in the Milky Way and M31 haloes.

While 4MOST will also survey hundred thousands of LMC and SMC stars and Milky Way halo stars (Cioni et al. 2019; Helmi et al. 2019; Christlieb et al. 2019), it is impossible to forecast their suitability for [Fe XIV] stacking experiments to constrain the hot-gas mass within the inner $\sim 50 \text{ kpc}$ of the Milky Way halo and the hot halo of the Magellanic Clouds (Lucchini, D’Onghia & Fox 2024) because of the complex stellar continua.

6. Summary and conclusions

In this paper, we have explored the possibility of studying the hot coronal gas of the Milky Way at $T \geq 10^6 \text{ K}$ by analyzing the highly forbidden solar coronal lines of [Fe X] and [Fe XIV] in the optical in absorption against bright extragalactic background sources. The main results of our study can be summarized as follows:

(1) Using an analytic model of the Milky Way’s coronal gas distribution, results from the HESTIA simulations of the Local Group, and constraints from FRB observations, we predict that the mean hydrogen column density for $T \geq 10^6 \text{ K}$ gas along a typical halo sightline from the Sun to the Galaxy’s virial radius is $N(\text{H}) \approx 5 \times 10^{20} \text{ cm}^{-2}$. Assuming the gas to be in a collisional ionization equilibrium and adopting an iron abundance half of the solar value, the expected Fe X and Fe XIV column densities are $\log N(\text{Fe X}) = 15.40$ and $\log N(\text{Fe XIV}) = 15.23$, where we expect non-thermal gas motions to dominate the Fe X and Fe XIV line widths.

(2) Based on the atomic data for the lines of [Fe X] $\lambda 6374.5$ and [Fe XIV] $\lambda 5302.9$, we predict characteristic equivalent widths for the coronal gas of $W_{6347} = 190 \mu\text{Å}$ and $W_{5302} = 220 \mu\text{Å}$. We investigate the typical velocity dispersion of the hot gas cells in the HESTIA simulation and from this generate synthetic absorption profiles of these extremely weak lines with and without noise. We conclude that a minimum S/N of $\sim 50,000$ is required to detect [Fe X] $\lambda 6374.5$ absorption at a 3σ level, while for [Fe XIV] $\lambda 5302.9$ the required S/N is $\sim 25,000$.

(3) We combine archival high-resolution spectral data of 739 AGN from VLT/UVES and KECK/HIRES to

construct a composite spectrum from stacking and to provide upper limits for $N(\text{Fe X})$ and $N(\text{Fe XIV})$ in the Milky Way halo. As expected, we do not find [Fe X] and [Fe XIV] absorption in the stacked spectrum, but obtain 3σ upper limits of $\log N(\text{Fe X}) \leq 16.27$ and $\log N(\text{Fe XIV}) \leq 15.85$. Our composite spectrum achieves a $S/N \approx 1,240$ near 5302 Å and ≈ 900 near 6374 Å . A feature near 6380 Å is clearly evident in the composite spectrum, the measured equivalent width being 29.5 mÅ . We identify this feature as a DIB in the foreground interstellar gas in the Milky Way disk.

(4) Finally, we discuss the possibility of detecting [Fe X] and [Fe XIV] absorption using new instruments and on-going/future observational campaigns. Our study implies that the up-coming extragalactic spectral surveys with millions of medium- to high-resolution optical spectra will provide an unprecedented wealth of absorption-line data that holds the prospect of detecting the extremely weak [Fe X] and [Fe XIV] lines in the Milky Way’s coronal gas, providing important information on the hot component of the Galaxy’s CGM and the total mass therein. With a somewhat higher oscillator strength, a spectral region not being contaminated by DIBs and telluric features, and a peak abundance near $2 \times 10^6 \text{ K}$, the [Fe XIV] $\lambda 5302.9$ line represents the most promising candidate to explore the coronal gas of the Milky Way with the “coronal lines” of iron.

Acknowledgements. This study makes extensive use of the SQUAD and KODIAQ spectral data libraries; we thank M.T. Murphy and J.M. O’Meara for sharing their data with us and providing helpful comments.

References

- Afruni, A., Pezulli, G., Fraternali, F., & Gronnow, A. 2023, MNRAS, 524, 2351
- Anderson, M.E. & Sunyaev, R. 2016, MNRAS, 459, 2806
- Anderson, M.E. & Sunyaev, R. 2018, A&A, 617, A123
- Asplund, M., Grevesse, N., Jacques Sauval, A., & Scott, P. 2009, ARA&A, 47, 481
- Bauer, F.E., Lira, P., Anguita, T., et al. 2023, The Messenger, 190, 34
- Ben Bekhti, N., Richter, P., Westmeier, T., & Murphy, M.T. 2008, A&A, 487, 583
- Ben Bekhti, N., Winkel, B., Richter, P., et al. 2012, A&A, 542, A110
- Bhattacharyya, J., Das, S., Gupta, A., Mathur, S., & Krongold, Y. 2023, ApJ, 952, 41
- Biaus, L., Nuza, S.E., Richter, P., et al. 2022, MNRAS, 517, 6170
- Bryans, P., Landi, E. & Savin, D.E. 2009, ApJ, 691, 1540
- Cioni, M.-R., L., Storm, J., Cameron, P.M. et al. 2019, The Messenger, 175, 54
- Crain, R.A. & van de Voort, F. 2023, ARA&A, 61, 473
- Christlieb, N., Battistini, C., Bonifacio, P. et al. 2019, The Messenger, 175, 26
- Comparat, J., Truong, N., Merloni, A., et al. 2022, A&A, 666, A156
- Cook, A.M., Bhardwaj, M., Gaensler, B.M., et al. 2023, ApJ, 946, 58
- Damle, M., Sparre, M., Richter, P., et al. 2022, MNRAS, 512, 3717

- Damle, M., Tonnesen, S., Sparre, M., & Richter, P. 2025, *ApJ*, 986, 69
- Das, S., Mathur, S., Gupta, A., & Krongold, Y. 2021, *ApJ*, 918, 83
- de Jong, R.S. 2019, *Nature Astronomy*, 3, 574
- D’Odorico, V., Christiani, S., Pomante, E., et al. 2016, *MNRAS*, 463, 2690
- D’Odorico, V., Bolton, J.S., Christensen, L., et al. 2024, *arXiv:2311.16803*
- Fang, T., Mckee C.F., Canizares, C.R., & Wolfire, M. 2006, *ApJ*, 644,174
- Fontana, A., & Ballester, P. 1995, *ESO Messenger*, 80, 3
- Fresco, A.Y., Péroux, C., Merloni, A., Hamanowicz, A., Szakacs, R. 2020, *MNRAS*, 499, 5230
- Fox, A.J., Richter, P., Wakker, B.P., et al. 2013, *ApJ*, 772, 111
- Fuhr, J.R., Martin, G.A., & Wiese, W.L. 1988, *J. Phys. Chem. Ref. Data*, 17, 1
- Gnat, O. & Sternberg, A. 2007, *ApJS*, 168, 213
- Grand, R.J.J., Gómez, F.A., Marinacci, F., et al. 2017, *MNRAS*, 467, 179
- Grottrian, W. 1939, *Naturwissenschaften*, 27, 214
- Guber, C.R. & Richter, P. 2016, *A&A*, 591, A137
- Guber, C.R., Richter, P. & Wendt, M. 2018, *A&A*, 609, A85
- Hani, M.H., Ellison, S.L., Sparre, M., Grand, R.J.J., Pakmor, R., Gomez, F.A., & Springel, V. 2019, *MNRAS*, 488, 135
- Helmi, A., Irwin, M., Deason, A., et al. 2019, *The Messenger*, 175, 23
- Hobbs, L.M. 1984, *ApJ*, 280, 132
- Hobbs, L.M. & Albert, C.E. 1984, *ApJ*, 281, 639
- Hobbs, L.M. 1985, *ApJ*, 298,357
- Hobbs, L.M., York, D.G., Snow, T.P., et al. 2008, *ApJ*, 680, 1256
- Hodges-Kluck, E.J., Miller, M.J., & Bregman, J.N. 2016, *ApJ*, 822, 21
- Jenniskens, P. & Desert, F.-X. 1994, *A&AS*, 106, 39
- Jin, S., Trager, S.C., Dalton, G.B. 2024, *MNRAS*, 530, 2688
- Kaaret, P., Koutroumpa, D., Kuntz, K.D., et al. 2020, *Nature Astronomy*, 4, 1072
- Klypin A., Kravtsov A.V., Bullock J.S., & Primack J.R. 2001, *ApJ*, 554, 903
- Kotuš, S.M., Murphy, M.T. and Carswell, R.F. 2017, *MNRAS*, 464, 3679
- Kramida, A., Ralchenko, Y., Reader, J., and the NIST ASD Team 2023, *NIST Atomic Spectra Database*, ver.5.11, online
- Krishnarao, D., Fox, A.J., D’Onghia, E., et al. 2022, *Nature*, 609, 58
- O’Meara, J.M., Lehner, N., Howk, J.C., et al. 2017, *AJ*, 154, 114
- Lan, T.-W., Ménard, B. & Zhu, G. 2015, *MNRAS*, 452, 3629
- Lehner, N., Savage, B. D., Richter, P., et al. 2007, *ApJ*, 658, 680
- Lehner, N., Howk, J.C., & Wakker, B.P. 2015, *ApJ*, 804, 79
- Lehner, N., Berek, S.C., Howk, J.C., et al. 2020, *ApJ*, 900, 9
- Li J.-T. & Bregman J.N. 2017, *ApJ*, 849, L105
- Liu, W., Chiao, M., Collier, M.R., et al. 2017, *ApJ*, 834 33
- Libeskind, N.I., Carlesi, E., Grand, R.J.J., et al. 2020, *MNRAS*, 498, 2698
- Locatelli, N., Ponti, G., Zheng, X., et al. 2024, *A&A*, 681, A78
- Lorimer, D.R., Bailes, M., McLaughlin, M.A., Narkevic, D.J., & Crawford, F. 2007, *Sci*, 318, 777
- Lucchini, S., D’Onghia, E. & Fox, A.J. 2024, *ApJ*, 967, L16
- Mainieri, V., Leibundgut, B., de Jong, R.S, et al. 2023, *The Messenger*, 190, 3
- Malaney, R.A. & Clampin, M. 1988, *ApJ*, 335, L57
- Maller, A.H., & Bullock, J.S. 2004, *MNRAS*, 355, 694
- Marasco, A., Fraternali, F., Lehner, N., & Howk, J.C. 2022, *MNRAS*, 515, 4176
- Marconi, A., Abreu, M., Adibekyan, V., et al. 2022, *SPIE*, 12184, 24
- Martynenko, N. 2022, *MNRAS*, 511, 843
- Merloni, A., Alexander, D.A., Banerji, B. et al., 2019, *The Messenger*, 175, 42
- Meyer, D.M. & Lauroesch, J.T. 1999, *ApJ*, 520, L103
- Miller, M.J., & Bregman, J.N. 2013, *ApJ*, 770, 118
- Miller, M.J., & Bregman, J.N. 2015, *ApJ*, 800, 14
- Murga, M., Zhu, G. Ménard, B. & Lan, T.-W. 2015, 452, 511
- Murphy, M.T., Kacprzak, G.G., Savorgnan, G.A.D., & Carswell, R.F. 2019, *MNRAS*, 482, 3458
- Naab, T. & Ostriker, J.P. 2017, *ARA&A*, 55, 59
- Navarro J.F., Frenk C.S., & White S.D.M. 1995, *MNRAS*, 275, 56
- Péroux, C. & Howk, J.C. 2020, *ARA&A*, 58, 363
- Péroux, C., Merloni, A., Liske, J. et al., 2023, *The Messenger*, 190, 42
- Pettini, M.,& D’Odorico, S. 1986, *ApJ*, 310, 700
- Pettini, M., Stathakis, R., D’Odorico, S., Molaro, P., & Vladilo, G. 1989, *ApJ*, 340, 256
- Predehl, P., Sunyaev, R.A., Becker, W. et al. 2020, *Nature*, 588, 277
- Prochaska, J.X., & Zheng, Y. 2019, *MNRAS*, 485, 648
- Putman, M.E.,Staveley-Smith, L., Freeman, K.C., et al. 2003, *ApJ*, 586, 170
- Richter, P., Savage, B.D., Wakker, B.P., Sembach, K.R., & Kalberla, P.M.W. 2001, *ApJ*, 549, 281
- Richter, P., Sembach, K.R., & Howk, J.C. 2003, *A&A*, 405, 1013
- Richard, J., Kneib, J.-P., Blake, C. et al., 2019, *The Messenger*, 175, 50.
- Richter, P., Westmeier, T. & Brüns, C. 2005, *A&A*, 442, L49
- Richter, P., Savage, B.D., Sembach, K.R., & Tripp, T.M. 2006, *A&A*, 445, 827
- Richter, P., Fang, T., & Bryan, G. L. 2006, *A&A*, 451, 767
- Richter, P., Krause, F., Fechner, C., Charlton, J.C., & Murphy, M.T. 2011, *A&A*, 528, A12
- Richter, P. 2012, *ApJ*, 750, 165
- Richter, P., Fox, A. J., Wakker, B. P., et al. 2013, *ApJ*, 772, 111
- Richter, P., Fox, A.J., Ben Bekhti, N., Murphy, M.T., Bomans, D., & Frank, S. 2014, *AN*, 335, 92
- Richter, P., Nuza, S. E., Fox, A. J., et al. 2017, *A&A*, 607, A48
- Richter, P. 2017, *ASSL*, 430, 15
- Richter, P. 2020, *ApJ*, 892, 33
- Rünger, F., Sparre, M., Richter, P., et al. 2025, *A&A*, in press
- Sarkar, K.C. 2024, *A&ARv*, 32, 1
- Savage, B.D., Sembach, K.R., Wakker, B.P., et al. 2003, *ApJS*, 146, 125
- Sembach, K.R., Wakker, B.P., Savage, B.D., et al. 2003, *ApJS*, 146, 165

- Shirai, T., Sugar, J., Musgrove, A., & Wiese, W.L. 2000, J. Phys. Chem. Ref. Data, Monograph No. 8
- Spitzer, L., Jr. 1956, ApJ, 124,20
- Springel, V. 2010, MNRAS, 401, 791
- Sutherland, R.S. & Dopita, M.A. 1993, ApJS, 88, 253
- Tepper-García, T., Richter, P., Schaye, J., Booth, C.M., Dalla Vecchia, C., & Theuns, T. 2012, MNRAS, 425, 1640
- Tepper-García, T., Richter, P., & Schaye, J. 2014, MNRAS, 436, 2036
- Tripp, T.M., Sembach, K.R., Bowen, D.V., et al. 2008, ApJ, 177, 39
- Tumlinson, J., Peebles, M.S. & Werk, J.K. 2017, ARA&A, 55, 389
- Wampler, E.J., Chen, J.S. & Setti, G. 1991, A&A, 248, 633
- Wang, Q., Hamilton, T. & Helfand, D.J. 1989, Nature, 341, 309
- White, S.D.M. & Frenk, C.S. 1991, 379, 52
- York, D.G. & Cowie, L.L. 1983, ApJ, 264, 49
- Zastrocky, T.W., Howk, J.C., Lehner, N., & O'Meara, J.M. 2018, AARN, 2, 227